RSC Advances

MnO2/carbon nanowalls electrode for future energy storage application: effect of carbon nanowalls growth period and MnO2 mass loading

Journal:	*RSC Advances*
Manuscript ID:	RA-ART-02-2014-001132.R1
Article Type:	Paper
Date Submitted by the Author:	04-Apr-2014
Complete List of Authors:	Abd El-Moneim, Ahmed; Egypt-Japan University of Science and Technology, Materials Science and Engineering Department hassan, Sameh; faculty of science, physic department suzuki, masaaki; Tokyo Institute of Technology, Department of Chemical Engineering Mori, Shinsuke; Tokyo Institute of Technology, Department of Chemical Engineering

RSC Advances

RSC Publishing

ARTICLE

MnO_2/carbon nanowalls electrode for future energy storage application: effect of carbon nanowalls growth period and MnO_2 mass loading

Cite this: DOI: 10.1039/x0xx00000x

Received 00th January 2012,
Accepted 00th January 2012

DOI: 10.1039/x0xx00000x

www.rsc.org/

Sameh Hassan,[bd] Masaaki Suzuki,[a] Shinsuke Mori,[a] and Ahmed Abd El-Moneim*[bc]

Nanostructured MnO_2 films with 50 and 100 µg cm^{-2} mass loadings supported on two dimensional (2D) stand–free carbon nanowalls (CNWs) were synthesized by anodic electrodeposition and investigated for supercapacitor application. The underlying CNWs films of different growth periods, 12-24 sec, were grown first by microwave plasma enhanced chemical vapor deposition on three dimensional (3D) nickel foam substrate. Tailoring MnO_2/CNWs/Ni hybrid nanocomposite electrode with an optimized CNWs growth period of 18 sec and a MnO_2 loading of 50 µg cm^{-2} achieves the best capacitive performance; it exhibits specific capacitance of 1170 F g^{-1} at galvanostatic charging-discharging current density of 1 mA cm^{-2} and retains 110 % of its initial capacitance after 2000 cycles at current density of 3 mA cm^{-2}. The high density of atomic scale graphitic edges, large surface area with optimized defects and degree of crystallinity of CNWs in conjunction with an efficient utilization of MnO_2 nanoparticles facilitated rapid electron, ion transport and electrochemical cyclic stability, and hence offering the potential of the unique capacitive behavior. These results demonstrate an exciting commercial potential for high performance, environmentally friendly and low-cost electrical energy storage devices based on MnO_2/CNWs/Ni hybrid electrode.

Introduction

Supercapacitors have received a lot of attention as viable electrical energy storage devices due to their high power density and almost unlimited cycle life. Furthermore, they provide higher energy density than conventional capacitors while higher power density than batteries.[1, 2] However, supercapacitors often have low energy storage media which are mainly determined by the energy density and specific capacitance of electrode materials. Hence, it is highly desirable to improve the energy density as well as specific capacitance of electrode materials in supercapacitors to enable their use as a future primary storage sources.[3-5]

According to the energy stored mechanism in supercapacitors, two types exist namely the electrical double-layer capacitor and the pseudo-capacitor.[6, 7] The capacitance of the former arises from the separation of electrical charge which is associated with the buildup of an electrical double layer at the interface between electrode and electrolyte; therefore, it strongly depends on the surface area of the electrode accessible to the electrolyte. Carbon materials are a major material component for such type of capacitor. The capacitance of the latter is due to the reversible faradic transfer of charge between electrode and electrolyte, i.e. related to a change in the oxidation state of the electrode. Transition metal oxides are major material components for such type of capacitor.

Due to their excellent electrocatalytic activity than carbon materials, transition metal oxides have been extensively used in many electrochemical applications including supercapacitors during the past decades.[8-21] MnO_2, compared to the other transition metal oxides, is the most thoroughly investigated for pseudocapacitors on the basis of its high theoretical specific capacitance of 1370 F g^{-1}, relatively low cost and environmentally benign nature.[22-27] Being limited by its poor electrical conductivity, the theoretical specific capacitance of MnO_2 has rarely been achieved in any experiment.[22] Fabricating ultrathin film (tens to hundreds of nanometers thick) of different MnO_2 loadings has been examined as one possible track to improve the electrical conductivity and deliver very high specific capacitances, within 700-1000 F g^{-1} range in aqueous solution.[27] Nevertheless, ultrathin film of MnO_2 electrode material has limitations with the lack of structural, chemical and mechanical stabilities, long-term cyclability, and low rate-capacity.[27] Hence, the most important basic challenge to adapt MnO_2-based supercapacitor for commercial application is to improve its energy density, via approaching specific capacitance close to that of its theoretical specific capacitance of 1370 F g^{-1}, while keeping a high power density and a long cycle life.

For improving the poor electronic conductivity, structural, chemical and mechanical stabilities of MnO_2 electrodes, considerable research efforts have been dedicated to tailor the electrode architecture via applying an ultrathin layer of MnO_2 on the surface of a porous, high surface area and electronically conducting structure such as carbon nanotubes,[28-31] graphene,[32,33] and organic matter[34-37] to shorten the solid state transport for ions and diffusion path lengths of electrons. This can produce a good electrochemical

performance without sacrificing the mass-loading of the MnO_2 phase.

Recently, microwave plasma-enhanced chemical vapor deposition (MPECVD) is among the early methods to synthesize vertically standing few layer graphenes or graphene nanowalls (GNWs).[38-42] GNWs can be described as self-assembled, vertically standing, few-layered graphene sheet nanostructures, which are also called as carbon nanowalls (CNWs), carbon nanosheets, and carbon nanoflakes. The CNWs form a self-supported network of wall structures with thicknesses and height ranging from a few nanometers to a few tens of nanometers according to the applied growth period during the fabrication process of CNWs. CNWs have a high density of atomic scale graphitic edges that are potential sites for electron field emission, which might lead to the application in flat panel displays and light sources.[38-42] The large surface area of CNWs was useful templates for the fabrication of other types of nanostructured materials in the field of electrochemistry including electrode for fuel cell and electrochemical sensors.[39-43]

To date scarce works have reported on the use of two dimensional CNWs architecture as template for an efficient utilization of insulating MnO_2 for supercapacitive application. The present work is undertaken to tailor a MnO_2/CNWs composite electrode with superior properties for supercapacitive application. Particular attention is given to the effect of the growth period of CNWs and level of MnO_2 mass loading.

Experimental

Growth of CNWs

The MPECVD system used in this study is a modified ASTeX DPA25 plasma applicator in which the quartz discharge tube of 15 mm inner diameter is utilized. The maximum power of microwave source is 250 W. Nickel foam is used as electron conductor 3D substrate with apparent surface area 1 cm^2. The applied parameters of the CNWs growth process are as follows: total flow rate, 50 sccm; CO flow rate, 46 sccm; H_2 flow rate, 4 sccm; total pressure, 250 Pa; microwave power, 80 W. The selected growth period during steady–state growth process is varied from 12-24 sec. During growth process, the substrate is placed at the centre of the applicator and heated up by the microwave discharge. Substrate temperature is monitored by the radiation thermometer (Japan Sensor TMZ9) and it is about 700°C during the growth process. In fact the utilization of Ni foam as a substrate for the deposition of CNWs process offers a more feasible process for the fabrication of CNWs in a very short time, a few tens of seconds. The things in common in other reports are that there is an induction period of 1–5 min before the onset of vertical graphene growth on the surface of Si and SiO_2 substrates.[38]

Electrochemical deposition of MnO_2

The electrochemical deposition of MnO_2 is carried out in 0.25 M $(CH_3COO)_2$ $Mn.4H_2O$ electrolyte via anodic deposition at 1 Volt using three electrodes cell. An Ag/AgCl used as a reference electrode (KCl saturated), Pt-rod as a counter electrode and the pre-prepared CNWs/Ni foam as a working electrode. The mass loading of the MnO_2 is controlled by adjusting the total charge passed through the electrode during deposition process and selected to be 50 and 100 µg cm^{-2}.

Structure and electrochemical characterizations of MnO_2/CNWs/Ni hybrid composite electrodes

The microstructure of the deposited films was studied using Hitachi S-4500 scanning electron microscope (SEM) and transmission electron microscopy (TEM) complement with energy dispersive X-ray (EDX), JEOL JEM-2010F. NRS-2100 Raman spectrometer with 514.5 nm wavelength incident laser light was used to analyse the underlying carbon deposits.

The electrochemical properties of the electrodes have been conducted in 0.5 M Na_2SO_4 electrolyte using three electrodes cell configuration. The cyclic voltammetry (CV), galvanostatic charge–discharge, and electrochemical impedance spectroscopy (EIS) studies have been performed using VersaSTAT3 potenitostat/galvanostat electrochemical system.

The CV behaviors were carried out within a potential range of 0–0.9 V vs. Ag/AgCl (KCl saturated) at scan rates of 10–300 mV s^{-1}. Galvanostatic charge/discharge cycling was conducted at constant current densities of 1–10 mA cm^{-2} between 0–1 V. The cycle life test was performed at current density of 3 mA cm^{-2} for 2000 cycles. The applied alternating current amplitude for EIS measurements was 10 mV root mean square in a frequency range of 0.1 Hz to 7 kHz.

Cyclic voltammetry specific capacitance (C_{sp}) was calculated from dividing the capacitive charge (Q), obtained using half the integrated area of the CV curve, by the film mass (m) and the width of the potential window (V) using equation (1):

$$C_{sp} = \frac{Q}{m.V} \qquad (1)$$

Chronopotentiometry discharge C_{sp} values were calculated by using charge-discharge current (I), potential change with discharge time (dV/dt) and the mass of the deposited film according to the equation:

$$C_{sp} = \frac{I.dt}{m.dV} \qquad (2)$$

The energy and power densities of a supercapacitor are generally of most importance for its rating as electrochemical power device. The energy density (E) and power density (P) of a supercapacitor are given by:

$$E = \frac{C_{sp}.V^2}{2} \qquad (3)$$

$$P = \frac{V^2}{4m.R} \qquad (4)$$

Where, R is the equivalent series resistance (ESR) of the capacitor.

Results and discussion

Structure and morphology of MnO_2/CNWs films

Fig. 1 shows SEM images of the MnO_2-free CNWs deposited films with different growth periods of 12 (a), 18 (b), and 24 (c) sec. The images show the growth of the two-dimensional carbon sheets

with honeycomb structure on the Ni substrate. In addition to the vertically standing maze-like structure, isolated very thin nanosheets, less aligned petal-like, highly branched type, and a kind of porous film have been fabricated so far. The increase in the growth period during the steady-state growth makes the carbon nanosheets higher, wavier and more crowded, while the thickness remains saturated.[37,42]

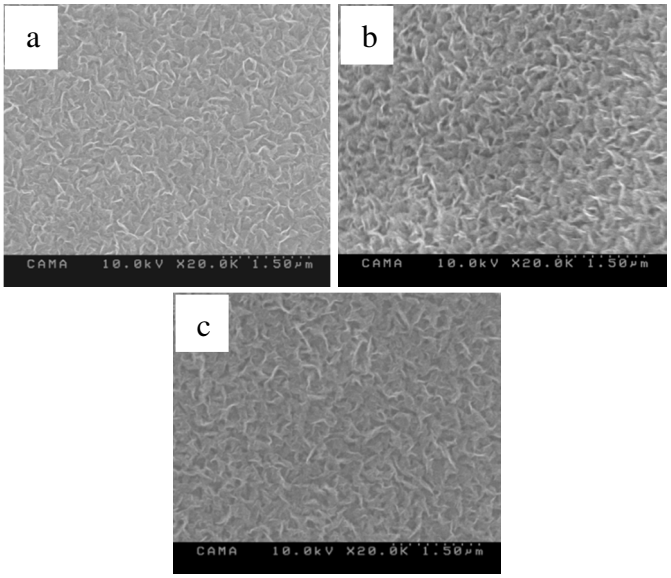

Fig. 1: SEM images of CNWs with growth periods of 12 (a), 18 (b), and 24 (c) sec.

Fig. 2 depicts TEM images of MnO_2-free CNWs film with growth period of 18 sec at different magnifications. The images confirm the 2D configuration of the nanowalls, which consists of crumpled and folded nano-domains of tens of nanometers in size, Figs. 2(a,b). The individual walls have rather wavy structures and their growth directions are oriented perpendicularly to the nickel substrate, thereby favouring electrical conduction from the substrate. It is also observed that the leading exposed reactive edges of the vertically grown CNWs tend to curl after reaching non-detectable certain height, Fig. 2 (b). The amount of apparent curl edges revealed to be increased with increasing the growth period of CNWs, in an indication for the reduction in the density of the upward exposed atomic graphitic edges. Finally, the high resolution TEM image shown in Fig. 2(c) reveals the presence of multilayers graphene, which indicates the graphitized structure of the CNWs. Furthermore, the spacing between neighbouring graphene layers is measured as approximately 0.34 nm, which corresponds to the reported one for CNWs and that of graphite (002) planes of graphite structures.[37,42]

The structure within the walls was also studied by Raman spectroscopy. Fig. 3 presents Raman spectra of carbon deposits in the MnO_2/CNWs films with CNWs growth periods of 12 (a), 18 (b) and 24 (c) sec. In general, Raman spectra consist of two main bands typical characteristic of carbon material, a D-band at 1360 cm^{-1} and G-band at 1590 cm^{-1}.[44-46] The detected D-band is attributed to defects due to the finite crystallite size or edges of graphene layers; while the G-band represents the in-plane bond-stretching motion of the pairs of carbon sp^2 atoms which indicates the presence of crystalline graphene layers.

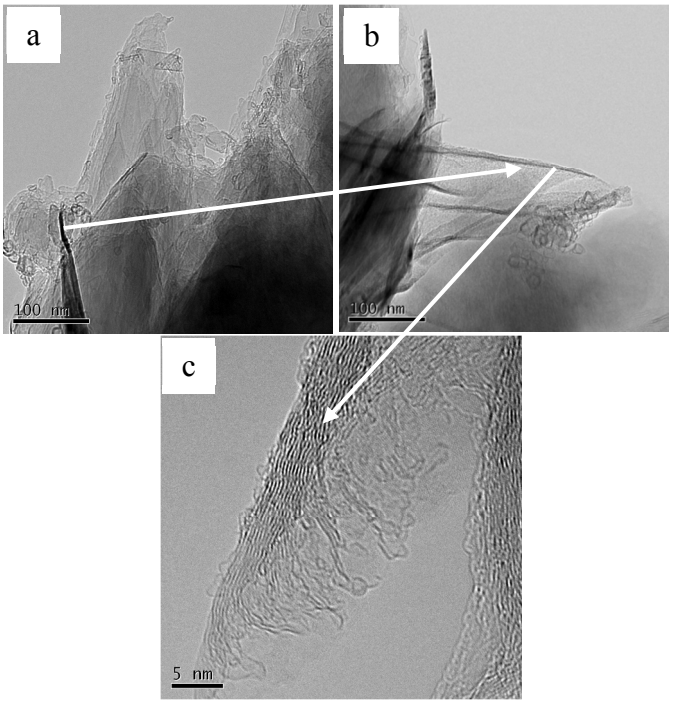

Fig. 2: TEM images of MnO_2-free CNWs film with growth period of 18 sec at different magnifications.

In addition, a small peak is observed at about 1620 cm^{-1}. This band corresponds to D′-band, indicating the disorder and associated with finite-size graphite crystals and graphene edges. This D′-band peak is also typical in the Raman spectra of CNWs.[44] The strong D-band peak and D′-band peak suggest presence of more nanocrystalline structure, graphene edges and defects such as distortion, vacancies and straining to graphitic lattices, which are prevalent features of CNWs.[38-44]

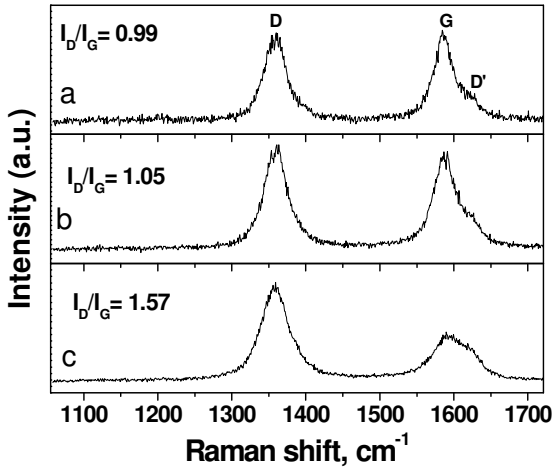

Fig. 3: Raman spectra of carbon deposits in MnO_2/CNWs electrode architectures with MnO_2 mass loading of 50 µg cm^{-2} and CNWs growth periods of 12 (a), 18 (b) and 24 (c) sec.

Quantitatively, the intensity ratio of D-band to G-band peaks (I_D/I_G) presents an excellent probe for monitoring the defect concentration and/or degree of crystallinity in the CNWs.[44] The lower ratio is a signature for lower defects concentration and/or higher degree of crystallinity in the CNWs structure. The intensity ratios of I_D/I_G for the MnO_2/CNWs electrodes with CNWs growth periods of 12, 18

and 24 sec are estimated to be 0.99, 1.05 and 1.57, respectively. This tendency agrees with the morphology changes shown in Figs. 1 and 2, in which CNWs become wavier and curl with growth period, revealing more defect in the graphite structure. It's worth to mention that the presence of defects and active edges in the graphitic lattices of carbon materials are prerequisites for supporting the nucleation and growth processes of the assembled electroactive nanoparticles and subsequently their service life.[38]

In accordance with the results presented in Figs. 1-3, CNWs have a little support on the Ni substrate and hence it is generally expected to retain most of their electronic properties and large amount of the exposed upward reactive edge planes and surface area. To meet and optimize these unique properties of CNWs with the pseudocapacitive characteristics of MnO_2, CNWs templates of different growth periods were decorated with MnO_2 at loading levels of 50 and 100 μg cm^{-2} via anodic electrodeposition.

Fig. 4 shows SEM images of CNWs-free MnO_2 film (a) and the MnO_2/CNWs films with MnO_2 mass loading of 50 μg cm^{-2} and CNWs growth periods of 12 (b), 18 (c) and 24 (d) sec. In comparison, the image of CNWs-free MnO_2 film Fig. 4(a) shows smooth surface with continuous cracks due to drying shrinkage, while the morphology of MnO_2 films deposited on CNWs, Figs. 4(b-d), composed of aggregates in the form of tangled porous microstructure follows the structure texture of the underlying CNWs film. The increase in the growth period of CNWs makes the tangled microstructure of the deposited MnO_2 continuous with less porous nature.

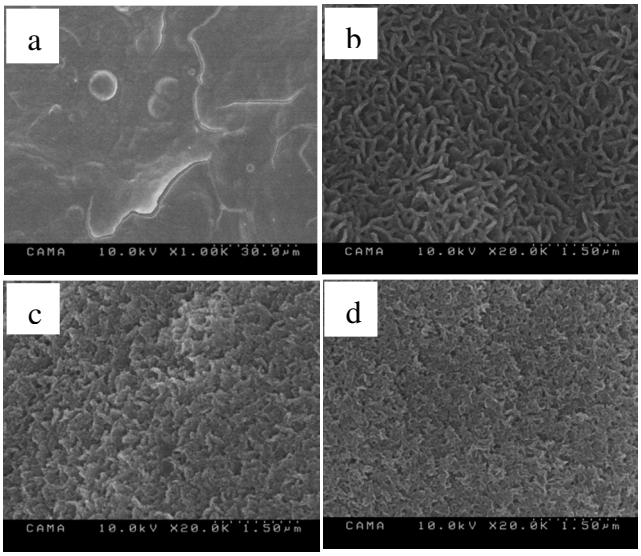

Fig. 4: SEM images of CNWs-free MnO_2 film (a) and the MnO_2/CNWs films with MnO_2 mass loading is 50 μg cm^{-2} and CNWs growth period of 12 (b), 18 (c) and 24 (d) sec.

Fig. 5 depicts TEM images of MnO_2/CNWs film with MnO_2 mass loading of 100 μg cm^{-2} and CNWs growth period of 18 sec, at different magnifications. The images clearly reveal that the MnO_2 nanodomains in the forms light and dark grey clusters (white circles) are randomly dispersed throughout the body, interlayer spacing, and more likely the exposed reactive edge planes of the stand-free graphene layers. In fact, it is difficult to treat the entire surface of CNWs with MnO_2 film from a liquid phase, because of the high surface tension, in homogeneities in defect distribution and narrow interspaces between the layers of CNWs.

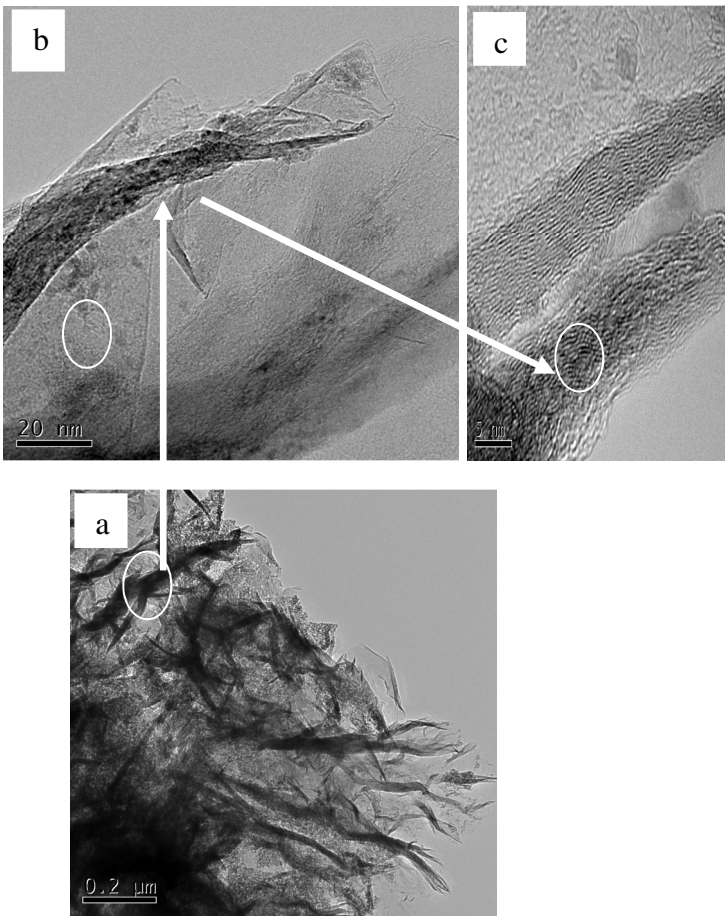

Fig. 5: TEM images of MnO_2/CNWs film with MnO_2 mass loading of 100 μg cm^{-2} and CNWs growth period of 18 sec at different magnifications.

Fig. 6 illustrates HRTEM images for CNWs-free MnO_2 (a) and the MnO_2/CNWs films with MnO_2 mass loading of 100 μg cm^{-2} and CNWs growth periods of 12 (b), 18 (c) and 24 (d) sec. As can be seen, the MnO_2 polymorph birnessite (white circles) is clearly visible in the image of CNWs-free MnO_2 film, Fig. 6 (a). The MnO_2 polymorph birnessite tends to diminish with the deposition on the CNWs template and almost disappears with deposition on CNWs template with growth period of 18 sec, Fig. 6(c), i.e. the formation of complete amorphous structure. This indicates that the CNWs enable the grain refinement of the MnO_2 structure. The formation of materials in an amorphous structure is generally preferable for supercapacitor and sensing applications due to the large accessible surface area and easy penetration of ions through the bulk of active materials.[36] It's also worth noting that CNWs still maintain the original lattice structure of the nanocrystallized graphene layers even after the deposition of MnO_2. The elemental analysis via EDX analysis technique at the nanoscopic level of Fig. 4(c) reveals high intensity ratio of C/Mn in the recorded EDX spectrum shown in Fig. 7. These observations confirm the fine assembly of ultra-thin MnO_2 film on the CNWs templates and development of electrode with high aspect ratio. In turn, the MnO_2/CNWs electrode is expected to retain high electronic conductivity, electrochemical stability and mechanical strength upon cycling thus provides an opportunity to tune the electrode material for optimal capacitive performance.

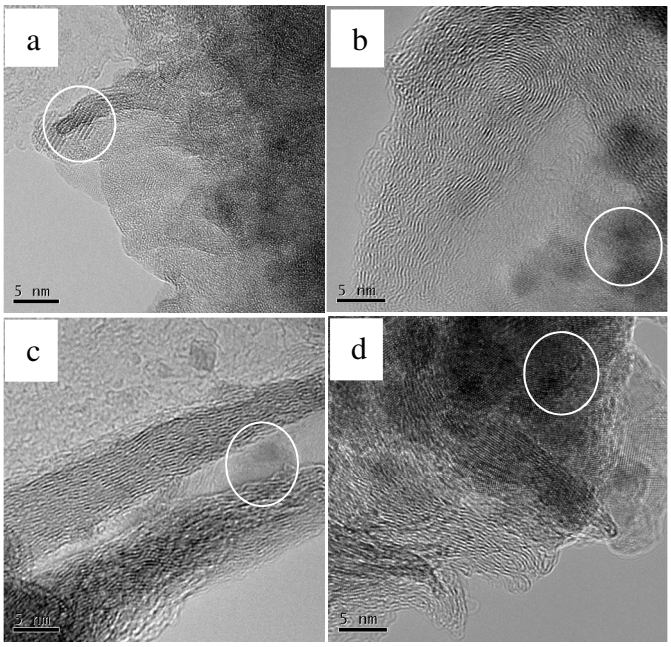

Fig. 6: HRTEM images for CNWs-free MnO_2 (a) and the MnO_2/CNWs films with MnO_2 mass loading of 100 μg cm^{-2} and CNWs growth periods of 12 (b), 18 (c) and 24 (d) sec.

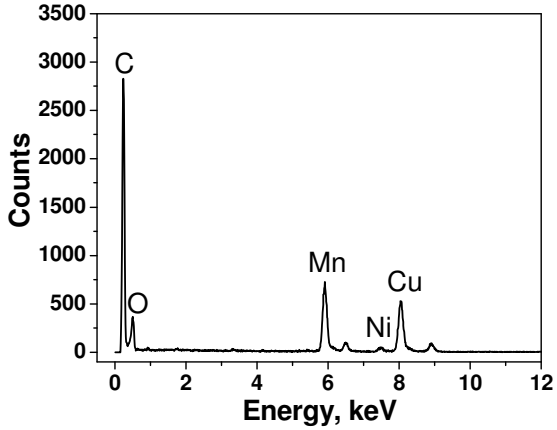

Fig. 7: EDX pattern of MnO_2/CNWs electrode with MnO_2 mass loading of 100 μg cm^{-2} and CNWs growth period of 18 sec.

Cyclic voltammetry and galvanostatic charge-discharge characteristics

The effects of different MnO_2 mass loadings and CNWs growth periods on the capacitive performance of MnO_2/CNWs electrodes are described in this section.

Fig. 8 shows the CV comparison curves for MnO_2-free CNWs (a), CNWs-free MnO_2 (b), and the MnO_2/CNWs electrodes with MnO_2 mass loading of 50 μg cm^{-2} and CNWs growth periods of 12 (c), 18 (d) and 24 (e) sec measured in 0.5 M Na_2SO_4 electrolyte at a scan rate of 90 mVs^{-1}. It is shown that the capacitive contributions of the MnO_2-free CNW (a) is negligible compared with CNWs-free MnO_2 (b) and MnO_2/CNWs (c-e) electrodes. The CV curves of CNWs-free MnO_2 and MnO_2/CNWs electrodes show nearly rectangular shape and characteristic mirror-image without clear redox peaks, indicative of highly capacitive behaviour with good ion response. Meanwhile, the MnO_2/CNWs electrodes show the larger integrated areas of the CV curves than that of CNWs-free MnO_2 electrode and hence, they have the higher C_{sp}.

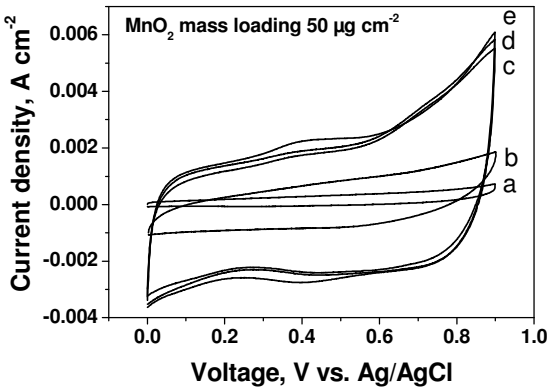

Fig. 8: CV curves for MnO_2-free CNWs (a), CNWs-free MnO_2 (b), MnO_2/CNWs electrode architectures with CNWs growth periods of 12 (c), 18 (d) and 24 (e) sec measured in 0.5 M Na_2SO_4 solution at a scan rate of 90 $mV\ s^{-1}$.

Figs. 9 and 10 summarizes the variation in the C_{sp} of CNWs-free MnO_2 (a) and the MnO_2/CNWs electrodes (b-d) with MnO_2 mass loading of 50 and 100 μg cm^{-2}, respectively, and CNWs growth periods of 12 (b), 18 (c) and 24 (d) sec. Both figures show a typical gradual decrease in the C_{sp} of all electrodes with the increase in the scan rate. The highest C_{sp} values obtained at MnO_2 mass loading of 50 μg cm^{-2} (Fig. 9) for CNWs-free MnO_2 (a) and MnO_2/CNWs electrodes with CNWs growth periods of 12 (c), 18 (d), and 24 (e) sec, at a scan rate of 10 $mV\ s^{-1}$, are 425, 1009, 1054, and 1030 F g^{-1}, respectively, and those at MnO_2 mass loading of 100 μg cm^{-2} (Fig. 10) are 488, 508, 685, and 533 F g^{-1}, respectively.

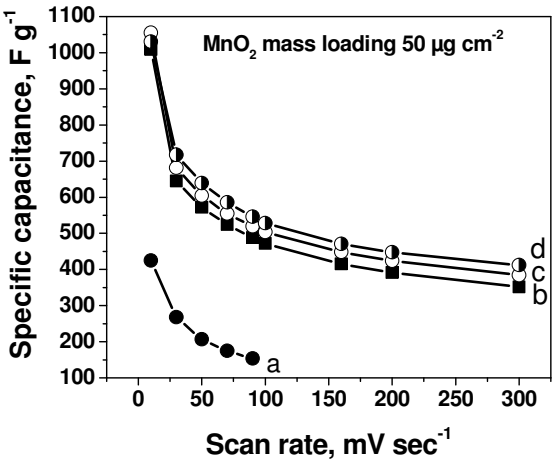

Fig. 9: C_{sp} versus scan rate for CNWs-free MnO_2 (a) and the MnO_2/CNWs electrodes with MnO_2 mass loading of 50 μg cm^{-2} and CNWs growth periods of 12 (b), 18 (c) and 24 (d) sec.

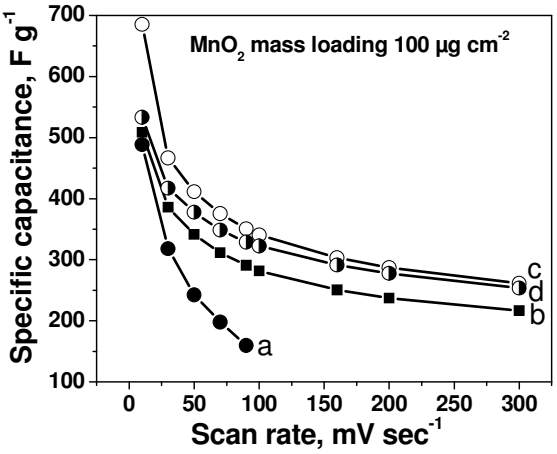

Fig. 10: C_{sp} versus scan rate for CNWs-free MnO_2 (a) and the MnO_2/CNWs electrodes with MnO_2 mass loading of 100 µg cm^{-2} and CNWs growth periods of 12 (b), 18 (c) and 24 (d) sec.

To further clarify and confirm the effect of CNWs and MnO_2 mass loading on the capacitive behavior and rate capability of electrodes, the charge-discharge profiles were measured by chronopotentiometry. Fig. 11 shows charge-discharge profiles of MnO_2-free CNWs (a), CNWs-free MnO_2 (b), and MnO_2/CNWs electrodes with MnO_2 mass loading of 50 µg cm^{-2} and CNWs growth periods of 12 (c), 18 (d) and 24 (e) sec measured in 0.5 M Na_2SO_4 electrolyte at current density of 1 mA cm^{-2}. In principle, the discharge profile of any oxide film with capacitive characteristics is basically consisted of three parts: a resistive component from sudden voltage drop (IR drop) due to the internal resistance of the deposited film, the capacitance component related to the voltage change due to ion separation in the double layer region at the electrode interface, and finally faradaic component in the longer time region due to charge transfer reaction of the film. As can be seen in Fig. 11, the IR drop for MnO_2-free CNWs (a) and CNWs-free MnO_2 (b) electrodes are significantly higher than those of MnO_2/CNWs electrodes indicating that the MnO_2/CNWs films have lower internal resistance than MnO_2-free CNWs and CNWs-free MnO_2 films. Among MnO_2/CNWs electrodes, the electrode with CNWs growth period of 18 sec has the highest C_{sp} as it has longer discharge time.

Figs. 12 and 13 present the summary plots of specific capacitance versus current density for CNWs-free MnO_2 and MnO_2/CNWs electrodes with MnO_2 mass loading of 50 and 100 µg cm^{-2}, respectively, and CNWs growth periods of 12 (b), 18(c) and 24 (d) sec. In both figures, the discharge C_{sp} gradually decreases by applying high current density. The highest C_{sp} values obtained at MnO_2 mass loading of 50 µg cm^{-2} (Fig. 12) for CNWs-free MnO_2 (a) and MnO_2/CNWs electrodes with CNWs growth periods of 12 (b), 18 (c) and 24 (d) sec at current density of 1 mA cm^{-2} are 438, 1108, 1170 and 1138 F g^{-1}, respectively, and those at MnO_2 mass loading of 100 µg cm^{-2} (Fig. 13) are 643, 603, 851 and 624 F g^{-1}, respectively. This is in coincidence with the CV results presented in Figs. 9 and 10 and indicates that MnO_2/CNWs electrodes do not only show higher C_{sp} but also better capability rate of charge-discharge than CNWs-free MnO_2 electrode. More importantly, the C_{sp} values of all MnO_2/CNWs electrodes with MnO_2 mass loading of 50 µg cm^{-2}, particularly that with CNWs growth period of 18 sec, approach the theoretical C_{sp} value of MnO_2, that is 1370 F g^{-1}.[22] It can, therefore, be said that CNWs templates provide more active sites for an efficient assembly and utilization of MnO_2 as promising pseudo-capacitance material.

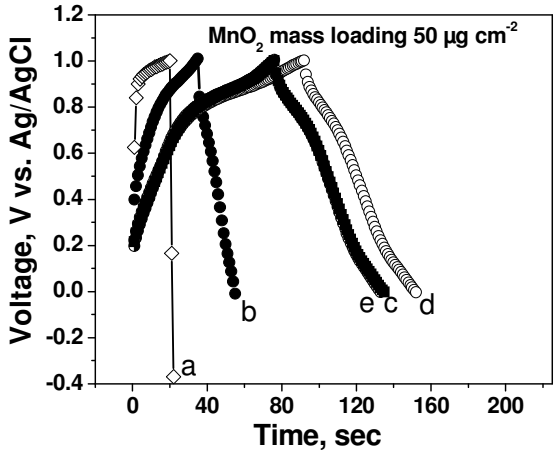

Fig. 11: Charge-discharge profiles of MnO_2-free CNWs (a), CNWs-free MnO_2 (b), and MnO_2/CNWs electrodes with MnO_2 mass loading of 50 µg cm^{-2} and CNWs growth periods of 12 (c), 18 (d) and 24 (e) sec measured in 0.5 M Na_2SO_4 electrolyte at current density of 1 mA cm^{-2}.

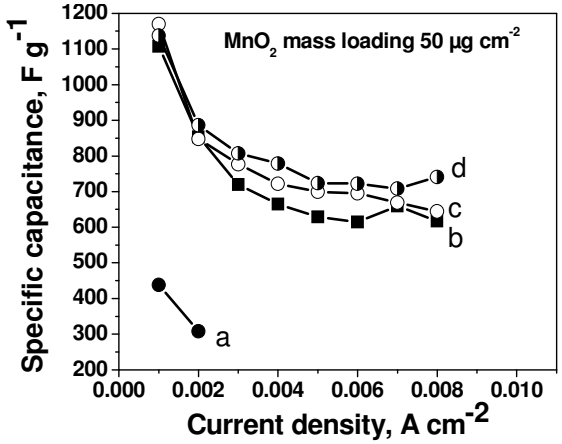

Fig. 12: C_{sp} versus current density for CNWs-free MnO_2 (a) and MnO_2/CNWs electrode architectures with MnO_2 mass loading of 50 µg cm^{-2} and CNWs growth periods of 12 (b), 18 (c) and 24 (d) sec.

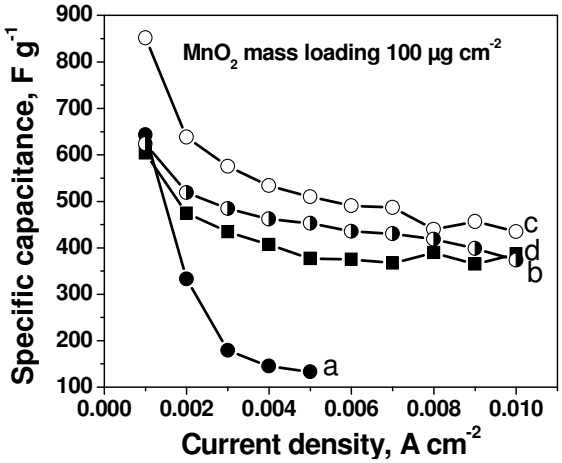

Fig. 13: C_{sp} versus current density for CNWs-free MnO_2 (a) and MnO_2/CNWs electrode architectures with MnO_2 mass loading of 100 µg cm^{-2} and CNWs growth periods of 12 (b), 18 (c) and 24 (d) sec.

Galvanostatic charge-discharge cyclic stability

Cycling performance is another key factor in determining the availability of supercapacitor electrodes for many practical applications. Excellent cycling stability is crucial for real supercapacitor operations.

Figs. 14 and 15 present the cycling performance of MnO_2/CNWs electrodes with MnO_2 mass loading of 50 and 100 μg cm^{-2}, respectively, and CNWs growth periods of 12 (b), 18 (c) and 24 (d) sec in 0.5 M Na_2SO_4 electrolyte by charging and discharging at 3 mA cm^{-2} for 2000 cycles. In general, the MnO_2/CNWs electrodes show a little decrease in the value of specific capacitance (down to range of 80-85 % of their initial values) during the initial 200-500 cycles and then the specific capacitance increased again up to 96-110 % (Fig. 14) and 85-92 % (Fig. 15) of their initial values after 2000 cycles. Specifically, the capacitance retention of MnO_2/CNWs electrodes with MnO_2 mass loading of 50 μg cm^{-2}, Fig. 14, and CNWs growth periods of 12 (a), 18 (b) and 24 (c) sec after 2000 cycles are 102, 110 and 96 %, respectively, and those at MnO_2 mass loading of 100 μg cm^{-2} are 86, 92 and 84 %, respectively, Fig. 15.

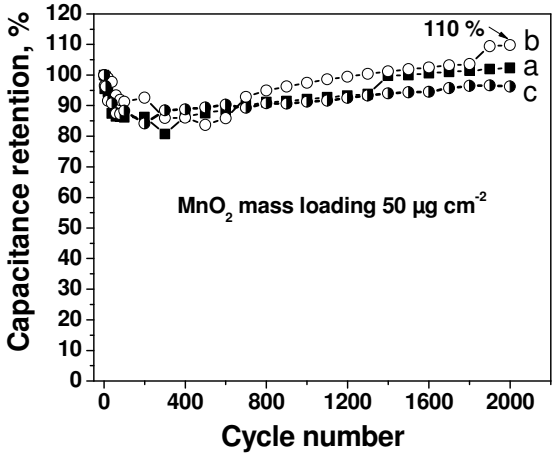

Fig. 14: Life-cycle data of MnO_2/ CNWs electrode architectures with MnO_2 mass loading of 50 μg cm^{-2} and CNWs growth periods of 12 (a), 18 (b) and 24 (c) sec, measured in 0.5 M Na_2SO_4 electrolyte at a current density of 3 mA cm^{-2}.

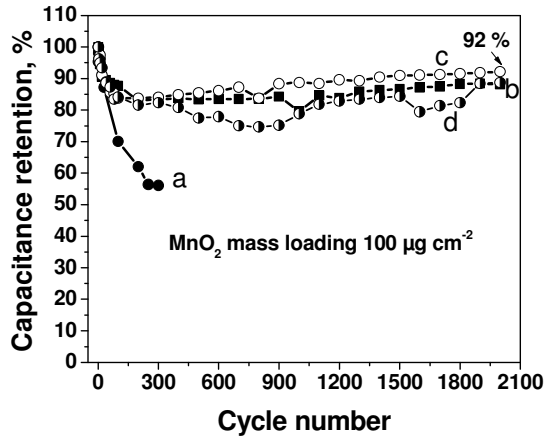

Fig. 15: Life-cycle data of CNWs-free MnO_2 (a) and MnO_2/ CNWs electrode architectures with MnO_2 mass loading of 100 μgcm^{-2} and CNWs growth periods of 12 (b), 18 (c) and 24 (d) sec, measured in 0.5 M Na_2SO_4 electrolyte at a current density of 3 mA cm^{-2}.

The surface morphology of MnO_2/CNWs electrode with MnO_2 mass loading of 50 μg cm^{-2} and CNWs growth period of 18 sec, which achieves the best capacitance retention, that is 110%, was characterized by SEM after 2000 cycles of charging-discharging, Fig. 16. Interestingly, the tangled morphology of as prepared MnO_2/CNWs electrode, Fig. 4 (c), is transformed after 2000 cycles to more open nanowalls structure that is finely decorated with MnO_2, particularly at its exposed upward active edges. This would provide a higher active surface area for ion accessibility with subsequent enhancement of the specific capacitance, i.e. electroactivation occurs.

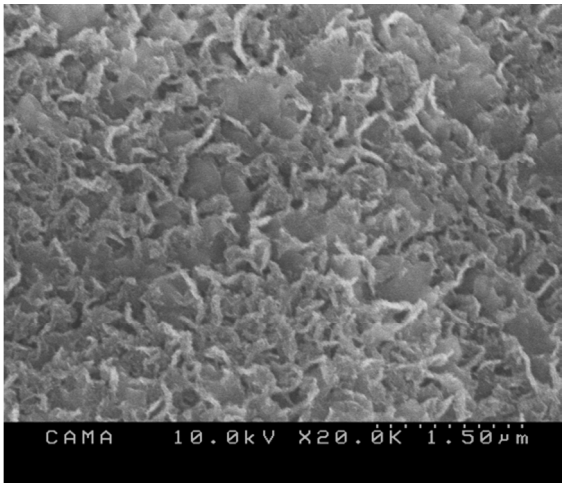

Fig. 16: SEM image of MnO_2/CNWs electrode with MnO_2 mass loading of 50 μg cm^{-2} and CNWs growth period of 18 sec after 2000 cycles of charging-discharging at 3 mA cm^{-2}.

Electrochemical Impedance Spectroscopy studies

In order to understand the reason behind the unique capacitive performance of the MnO_2/CNWs electrode compared to CNWs-free MnO_2 electrode, comparative electrochemical impedance spectroscopy (EIS) data were collected to quantify the electronic and ionic conductivities and diffusive behavior of the MnO_2-based films. Fig. 17 shows Nyquist plots for CNWs-free MnO_2 (a) and MnO_2/CNWs electrodes, with MnO_2 mass loading of 100 μg cm^{-2} and CNWs growth periods of 12 (b), 18 (c) and 24 (d) sec, measured in 0.5 M Na_2SO_4 electrolyte. In general, the impedance spectra of films used in supercapacitor application are composed of a high-frequency arc region followed by a low-frequency line.[47-51] The very high-frequency intercept at the real impedance part (Z′) at the beginning of the arc represents the equivalent series resistance (ESR), which includes the ionic resistance of the electrolyte, the intrinsic resistance of the active material, intrinsic resistance of current collector, and the contact resistance at the interface between active material and current collector. The power density of supercapacitors depends strongly on the ESR. The arc in the high-frequency region corresponds to the charge transfer resistance (R_{ct}) caused by the charge transfer process (Faradaic reactions) and double layer charging on the electrode surface. The magnitude of the R_{ct} can be derived from diameter of the arc. The line at lower frequency region is a result of ion diffusion/transport (Warburg resistance, W) through the pores of the deposited films, i.e. typical characteristics of porous electrodes.[48-50]

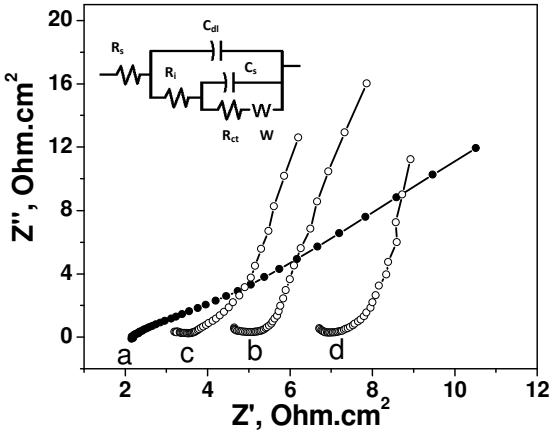

Fig. 17: The high frequency region of the recorded full impedance plots for CNWs-free MnO_2 (a) and MnO_2/CNWs electrode architectures with MnO_2 mass loading of 100 µg cm^{-2} and CNWs growth periods of 12 (b), 18 (c) and 24 (d) sec, measured in 0.5 M Na_2SO_4 electrolyte at 30^0C in the frequency range of 0.1 Hz–7 kHz at 10 mV amplitude. The inset is the equivalent circuit proposed for the fitting of the impedance data.

The impedance data presented in Fig. 17 were analysed using software provided with the electrochemical work station. The equivalent circuit model proposed for fitting the impedance data is the inset of Fig.17. The model consists of solution resistance, R_s, interface resistance, R_i, which represents ESR value, charge transfer resistance, R_{ct}, Warburg impedance, W, double layer capacitance, C_{dl}, and pseudo-capacitance, C_s.

The fitting results shows that the ESR values for CNWs-free MnO_2 (a) and MnO_2/CNWs electrodes, with CNWs growth periods of 12, 18 and 24 sec are 2.04, 4.65, 3.19, and 6.68 Ω, respectively. This refers that the contact resistance affects ESR with the presence of underlying CNWs compared with CNWs-free MnO_2 film. The R_{ct} values for CNWs-free MnO_2 and MnO_2/CNW electrodes with CNWs growth periods of 12, 18, and 24 sec are 3.28, 1.42, 1.02, and 1.92 Ω, respectively. The decrease in the R_{ct} value with presence of CNWs reflects the enhancement in the electronic and ionic conductivities of MnO_2 with the presence of CNWs. The optimal ESR and R_{ct} values are obtained with CNWs growth period of 18 sec and reduced with the reduction in the MnO_2 mass loading from 100 to 50 µg cm^{-2}. Besides, the slope of the Nyquist plots was found to increase with decreasing MnO_2 mass loading and/or the presence of CNWs, reflecting a decrease in the Warburg resistance (W) or fast electrolyte ion diffusion into the composite array.

In brief, the improvement in the capacitive performance is noticed not only with the presence of CNWs but also with the reduction in the MnO_2 mass loading. The presence of CNWs and low mass loading of MnO_2 create more active sites, facilitate the access of the electrolyte ions onto the surface of MnO_2 and makes electron transport between CNWs and MnO_2 easier as confirmed by the results obtained from EIS study. Finally, the energy density and power density values of MnO_2/CNWs electrodes estimated from the C_{sp} at charging-discharging current density of 1 mA cm^{-2} are in the range of 153.8-162.5 Wh/kg and 762.2-915.7 W/kg, respectively.

Conclusions

We have successfully developed new MnO_2/CNWs/Ni hybrid electrode materials for sueprcapacitor applications through two synthesis methods: MPECVD method that offers a feasible process for the fabrication of stand-free CNWs in a very short time, and anodic electrodeposition method for synthesizing nanoscopic MnO_2 film on CNWs architecture. Optimizing the growth period of CNWs by 18 sec and loading level of MnO_2 by 50 µg cm^{-2} lead to MnO_2/CNWs/Ni hybrid electrode with a superior capacitive behaviour among all electrodes examined so far for supercapacitor applications. Several unique characteristics of the MnO_2/CNWs/Ni hybrid electrodes make them promising candidates as high performance EC electrode materials include the following: (i) The stand-free graphene nanowalls on nickel foam current collector with a little support probably enable to retain nearly all of their inherent electronic properties; (ii) CNWs consists of nano-domains of a few tens of nanometers in size, and individual CNWs are found to have defects which support the nucleation and growth of MnO_2 nanoparticles and subsequently their cyclic stability; (iii) the unique architecture of stand-free CNWs reduces the diffusion length of ions within the pseudocapacitive phase ensuring an efficient utilization of the active materials; and (iv) Ensuring high C_{sp} of 1170 F g^{-1} at 1 mA cm^{-2}, a capacitance retention of 110 % after 2000 cycles at a current density of 3 mA cm^{-2}, energy density of 162.5 Wh/kg and power density of 915.7 W/kg. As a consequence, these unique characteristics demonstrate the exciting commercial potential for high performance, environmentally friendly and low-cost electrical energy storage devices based on this new MnO_2/CNWs/Ni hybrid material.

Acknowledgements

The authors gratefully acknowledge the Missions Sector-Higher Education Ministry, Egypt for financial support through this work, and Materials Science and Engineering department at E-JUST. We thank Mr. K. Hori and J. Koki of the Centre for Advanced Material Analysis in Tokyo Tech. for assistance with the TEM observations.

Notes and references

[a] Department of Chemical Engineering, Tokyo Institute of Technology, 2-12-1 O-Okayama, Meguro-ku, Tokyo, Japan, 152-8552.

[b]Material Science and Engineering Department, Egypt-Japan University of Science and Technology, New Borg El Arab City, Alexandria, Egypt, 21934.

† On leave from Physical Chemistry Department, National Research Centre, Cairo, Egypt.
Currently in Physics Department, Faculty of Science, Menoufiya University, Shebin El Kom, Egypt.
Corresponding author. Tel: +201281229082. E-mail: ahmed.abdelmoneim@ejust.edu.eg

1. B. E. Conway, *Electrochemical supercapacitors : scientific fundamentals and technological applications*, Plenum Press, New York [u.a.], 1999.

2. A.F. Burke, T.C. Murphy, D.H. Goughtly, B. Vyas, T. Takamura and J. R. H. (Eds.), Materials for electrochemical energy storage and conversion--batteries, capacitors, and fuel cells, Pittsburgh, Pa., 1995.

3. L. T. Lam and R. Louey, *Journal of Power Sources*, 2006, **158**, 1140-1148.

4. C.-C. Hu, K.-H. Chang, M.-C. Lin and Y.-T. Wu, *Nano Letters*, 2006, **6**, 2690-2695.

5. L. Cao, F. Xu, Y. Y. Liang and H. L. Li, *Advanced Materials*, 2004, **16**, 1853-1857.

6. M. Winter and R. J. Brodd, *Chemical reviews*, 2004, **104**, 4245-4269.

7. A. G. Pandolfo and A. F. Hollenkamp, *Journal of Power Sources*, 2006, **157**, 11-27.

8. L. Yuan, X.-H. Lu, X. Xiao, T. Zhai, J. Dai, F. Zhang, B. Hu, X. Wang, L. Gong, J. Chen, C. Hu, Y. Tong, J. Zhou and Z. L. Wang, *ACS Nano*, 2011, **6**, 656-661.

9. X. Xiao, T. Ding, L. Yuan, Y. Shen, Q. Zhong, X. Zhang, Y. Cao, B. Hu, T. Zhai, L. Gong, J. Chen, Y. Tong, J. Zhou and Z. L. Wang, *Advanced Energy Materials*, 2012, **2**, 1328-1332.

10. Q. Li, Z.-L. Wang, G.-R. Li, R. Guo, L.-X. Ding and Y.-X. Tong, *Nano Letters*, 2012, **12**, 3803-3807.

11. J. Liu, J. Jiang, C. Cheng, H. Li, J. Zhang, H. Gong and H. J. Fan, *Advanced Materials*, 2011, **23**, 2076-2081.

12. X. Lu, G. Wang, T. Zhai, M. Yu, J. Gan, Y. Tong and Y. Li, *Nano Letters*, 2012, **12**, 1690-1696.

13. C. Guan, J. Liu, C. Cheng, H. Li, X. Li, W. Zhou, H. Zhang and H. J. Fan, *Energy & Environmental Science*, 2011, **4**, 4496-4499.

14. A. A. El-Moneim and B. M. M., *International Journal of Electrochemical Science*, 2012, **7**, 671 – 685.

15. A. A. El-Moneim, *International Journal of Hydrogen Energy*, 2011, **36**, 13398-13406.

16. A. A. El-Moneim, J. Bhattarai, Z. Kato, K. Izumiya, N. Kumagai and K. Hashimoto, *ECS Transactions*, 2010, **25**, 127-137.

17. A. A. El-Moneim, K. Kumagai and K. Hashimoto, *Materials Transactions*, 2009, **66**, 1969-1977.

18. A. A. El-Moneim, N. Kumagai, K. Asami and K. Hashimoto, *Materials Transactions*, 2005, **46**, 309-316.

19. K. Hashimoto, A. A. El-Moneim, N. Kumagai and K. Asami, *ECS Transactions*, 2006, **1**, 491-497.

20. S. Hassan, M. Suzuki and A. Abd El-Moneim, *Electrical and Electronic Engineering*, 2012, **2**, 18-22.

21. S. Hassan, M. Suzuki and A. Abd El-Moneim, *American Journal of Materials Science*, 2012, **2**, 11-14.

22. M. Toupin, T. Brousse and D. Bélanger, *Chemistry of Materials*, 2004, **16**, 3184-3190.

23. A. E. Fischer, K. A. Pettigrew, D. R. Rolison, R. M. Stroud and J. W. Long, *Nano Letters*, 2007, **7**, 281-286.

24. G. Yu, L. Hu, M. Vosgueritchian, H. Wang, X. Xie, J. R. McDonough, X. Cui, Y. Cui and Z. Bao, *Nano Letters*, 2011, **11**, 2905-2911.

25. L. Hu, W. Chen, X. Xie, N. Liu, Y. Yang, H. Wu, Y. Yao, M. Pasta, H. N. Alshareef and Y. Cui, *ACS Nano*, 2011, **5**, 8904-8913.

26. L. Xingyou, H. Akihiko, F. Takeshi and C. Mingwei, *Nature Nanotechnology*, 2011, **6**, 232-236.

27. N. Nagarajan, M. Cheong and I. Zhitomirsky, *Materials Chemistry and Physics*, 2007, **103**, 47-53.

28. S.-B. Ma, K.-W. Nam, W.-S. Yoon, X.-Q. Yang, K.-Y. Ahn, K.-H. Oh and K.-B. Kim, *Journal of Power Sources*, 2008, **178**, 483-489.

29. S. R. Sivakkumar, J. M. Ko, D. Y. Kim, B. C. Kim and G. G. Wallace, *Electrochimica Acta*, 2007, **52**, 7377-7385.

30. S. W. Lee, J. Kim, S. Chen, P. T. Hammond and Y. Shao-Horn, *ACS Nano*, 2010, **4**, 3889-3896.

31. L. Hu, M. Pasta, F. L. Mantia, L. Cui, S. Jeong, H. D. Deshazer, J. W. Choi, S. M. Han and Y. Cui, *Nano Letters*, 2010, **10**, 708-714.

32. Q. Cheng, J. Tang, J. Ma, H. Zhang, N. Shinya and L.-C. Qin, *Carbon*, 2011, **49**, 2917-2925.

33. J. Yan, Z. Fan, T. Wei, W. Qian, M. Zhang and F. Wei, *Carbon*, 2010, **48**, 3825-3833.

34. R. Liu and S. B. Lee, *Journal of the American Chemical Society*, 2008, **130**, 2942-2943.

35. L. Chen, L.-J. Sun, F. Luan, Y. Liang, Y. Li and X.-X. Liu, *Journal of Power Sources*, 2010, **195**, 3742-3747.

36. S. Hassan, M. Suzuki and A. A. El-Moneim, *Journal of Power Sources*, 2014, **246**, 68-73.

37. X. Jin, W. Zhou, S. Zhang and G. Z. Chen, *Small*, 2007, **3**, 1513-1517.

38. M. Hiramatsu and M. Hori, *Carbon nanowalls : synthesis and emerging applications*, Springer, Wien; New York, 2010.

39. Y. Wu, P. Qiao, T. Chong and Z. Shen, *Advanced Materials*, 2002, **14**, 64-67.

40. K. Shiji, M. Hiramatsu, A. Enomoto, M. Nakamura, H. Amano and M. Hori, *Diamond and Related Materials*, 2005, **14**, 831-834.

41. Y. Wu, B. Yang, B. Zong, H. Sun, Z. Shen and Y. Feng, *Journal of Materials Chemistry*, 2004, **14**, 469-477.

42. S. Mori, T. Ueno and M. Suzuki, *Diamond and Related Materials*, 2011, **20**, 1129-1132.

43. S. Hassan, M. Suzuki, S. Mori and A. A. El-Moneim, *Journal of Power Sources*, 2014, **249**, 21-27.

44. K. Tanaka, M. Yoshimura, A. Okamoto and K. Ueda, *Japanese Journal of Applied Physics Part 1 Regular Papers Short Notes and Review Papers*, 2005, **44**, 2074-2076.

45. K. Kobayashi, M. Tanimura, H. Nakai, A. Yoshimura, H. Yoshimura, K. Kojima and M. Tachibana, *Journal of applied physics.*, 2007, **101**, 94306.

46. M. S. Dresselhaus, G. Dresselhaus, R. Saito and A. Jorio, *Physics reports*, 2005, **409**, 47.

47. Q. Lu and Y. Zhou, *Journal of Power Sources*, 2011, **196**, 4088-4094.

48. A. Celzard, F. Collas, J. F. Marêché, G. Furdin and I. Rey, *Journal of Power Sources*, 2002, **108**, 153-162.

49. T. Tüken, B. Yazıcı and M. Erbil, *Progress in Organic Coatings*, 2004, **50**, 115-122.

50. M. D. Stoller, S. Park, Y. Zhu, J. An and R. S. Ruoff, *Nano Letters*, 2008, **8**, 3498-3502..